arXiv:1402.6452v1 [gr-qc] 26 Feb 2014

Tests of Local Lorentz Invariance Violation of Gravity in the Standard-Model Extension with Pulsars

Lijing Shao*
Max-Planck-Institut für Radioastronomie, Auf dem Hügel 69, D-53121 Bonn, Germany
School of Physics, Peking University, Beijing 100871, China

Standard-model extension (SME) is an effective field theory introducing all possible Lorentz-violating (LV) operators to the standard model (SM) and general relativity (GR). In the pure-gravity sector of minimal SME (mSME), nine coefficients describe dominant observable deviations from GR. We systematically implemented twenty-seven tests from thirteen pulsar systems to tightly constrain eight linear combinations of these coefficients with extensive Monte Carlo simulations. It constitutes the first detailed and systematic test of the pure-gravity sector of mSME with the state-of-the-art pulsar observations. No deviation from GR was detected. The limits of LV coefficients are expressed in the canonical Sun-centered celestial-equatorial frame for convenience of further studies. They are all improved by significant factors of tens to hundreds with existing ones. As a consequence, Einstein's equivalence principle is verified substantially further by pulsar experiments in terms of local Lorentz invariance in gravity.

PACS numbers: 04.80.Cc, 11.30.Cp, 97.60.Gb

Introduction. Einstein's general relativity (GR) has passed all experimental scrutinies for almost one hundred years with flying colors [1, 2]. However, besides current puzzles on the nature of dark matter and dark energy, there exist difficulties to combine GR and the standard model (SM) into a unified theory. A full theory of quantum gravity (QG) may settle the issues, but such a theory is still missing. Although one expects that the full QG theory will *reduce to* or *emerge as* GR for the gravity interaction in our accessible energy regime, it may still leave *relic effects* as *QG windows* [3–18]. They are widely predicted by string theory, loop quantum gravity, and noncommutative field theories, wherein Lorentz-violating (LV) effects are well-known examples. Because of the importance of gravity, as a fundamental interaction, and Lorentz symmetry, as a fundamental property of spacetime, persistent efforts to probe possible LV deviations from GR are well justified and readily desired [3–20].

Recently, there is a strong belief that GR and SM are effective field theories (EFTs) of the underlying full theory [21]. With the fact that GR and SM have passed all tests up to now, one would expect that LV deviations, if any, would be supressed by a high energy scale. Hence it is natural to include extra terms in the context of EFTs. Standard-model extension (SME) is constructed as a convenient experimentally working framework to probe all possible LV deviations in the spirit of EFTs [3–6, 10–13, 15, 16].

In this Letter, for the first time, we systematically used various state-of-the-art pulsar observations to constrain LV effects in the pure-gravity sector of minimal SME (mSME) [13]. We improved all limits over previous ones [22–24] by substantial factors of tens to hundreds. Einstein's equivalence principle is thus verified further in terms of local Lorentz invariance in gravity. Light speed $c = 1$ is adopted throughout.

Pure-gravity sector of mSME. In SME, a general Lagrangian including gravity in Riemann-Cartan spacetime has the structure, $\mathcal{L} = \mathcal{L}_{\rm LI} + \mathcal{L}_{\rm LV}$, where $\mathcal{L}_{\rm LI}$ and $\mathcal{L}_{\rm LV}$ are Lorentz-invariant (LI) and LV terms respectively [11]. We focus on the limit of Riemannian spacetime and the pure-gravity sector with LV operators of only mass dimension four or less (the so-called mSME). Then $\mathcal{L}_{\rm LI} = \sqrt{-g}(R - 2\Lambda)/16\pi G$ is the usual Einstein-Hilbert action of GR, with g the derminant of the metric, R the Ricci scalar, and Λ the cosmological constant that is set to zero for localized systems. The LV Lagrangian at leading order reads [11, 13],

$$\mathcal{L}_{\rm LV} = \frac{\sqrt{-g}}{16\pi G}\left(-uR + s^{\mu\nu}R^{\rm T}_{\mu\nu} + t^{\kappa\lambda\mu\nu}C_{\kappa\lambda\mu\nu}\right) , \qquad (1)$$

where $R^{\rm T}_{\mu\nu}$ is the trace-free Ricci tensor and $C_{\kappa\lambda\mu\nu}$ is the Weyl conformal tensor. The LV fields, u, $s^{\mu\nu}$, and $t^{\kappa\lambda\mu\nu}$, violate both the *particle* local Lorentz invariance and the diffeomorphism, while the *observer* local Lorentz invariance is preserved. Because $s^{\mu\nu}$ and $t^{\kappa\lambda\mu\nu}$ inherit the symmetries of $R^{\rm T}_{\mu\nu}$ and $C_{\kappa\lambda\mu\nu}$ respectively, there exist in total twenty independent LV coefficients [13]. It is interesting to note that, if the symmetry breaking is spontaneous, SME coefficients arise from the underlying dynamics, so they must be regarded as dynamical fields. In contrast, if the breaking is explicit, the fields originate as prescribed spacetime functions that play no dynamical rôle. The geometry of Riemann-Cartan spacetime prohibits the later [11, 12]. Hence, only spontaneous breaking is considered here. After properly accounting for Nambu-Goldstone modes and adopting several plausible assumptions, Bailey and Kostelecký found that nine components of a trace-free matrix $\bar{s}^{\mu\nu}$, which are the (rescaled) vacuum expectation values of $s^{\mu\nu}$, describe dominant observable effects; see [13] for details.

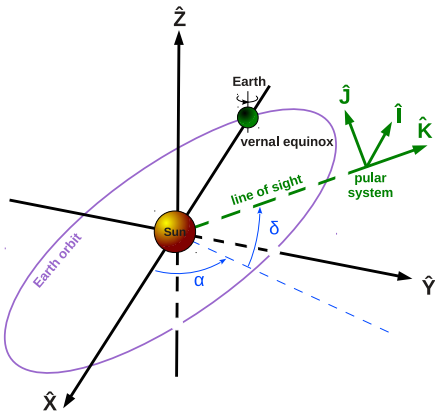

FIG. 1. The canonical spatial reference frame for SME is the Sun-centered celestial-equatorial frame $(\hat{\mathbf{X}}, \hat{\mathbf{Y}}, \hat{\mathbf{Z}})$, with $\hat{\mathbf{X}}$ pointing from the Earth to the Sun at vernal equinox, $\hat{\mathbf{Z}}$ along the rotating axis of the Earth, and $\hat{\mathbf{Y}} \equiv \hat{\mathbf{Z}} \times \hat{\mathbf{X}}$ [10]. The frame $(\hat{\mathbf{I}}, \hat{\mathbf{J}}, \hat{\mathbf{K}})$ is comoving with the pulsar system, with $\hat{\mathbf{K}}$ pointing along the line of sight to the pulsar, while $(\hat{\mathbf{I}}, \hat{\mathbf{J}})$ constitutes the sky plane with $\hat{\mathbf{I}}$ to east, and $\hat{\mathbf{J}}$ to north [25]. Besides a boost of $\mathcal{O}(10^{-3})$, these two frames are related by matrices $\mathcal{R}^{(\alpha)}$ and $\mathcal{R}^{(\delta)}$ [26]. $(\hat{\mathbf{I}}, \hat{\mathbf{J}}, \hat{\mathbf{K}})$ is denoted as $(\vec{e}_1, \vec{e}_2, \vec{e}_3)$ in [13].

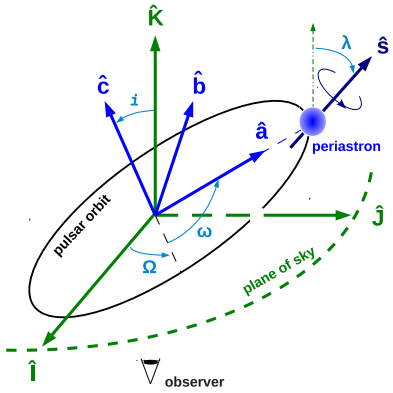

FIG. 2. The spatial frame $(\hat{\mathbf{a}}, \hat{\mathbf{b}}, \hat{\mathbf{c}})$ is centered at the pulsar system with $\hat{\mathbf{a}}$ pointing from the center of mass to the periastron, $\hat{\mathbf{c}}$ along the orbital angular momentum, and $\hat{\mathbf{b}} \equiv \hat{\mathbf{c}} \times \hat{\mathbf{a}}$. It is related to $(\hat{\mathbf{I}}, \hat{\mathbf{J}}, \hat{\mathbf{K}})$ frame through rotation matrices $\mathcal{R}^{(\Omega)}$, $\mathcal{R}^{(i)}$, and $\mathcal{R}^{(\omega)}$ [26]. The spin direction $\hat{\mathbf{S}}$ has a polar angle λ and an azimuthal angle η (not shown) in $(\hat{\mathbf{I}}, \hat{\mathbf{J}}, \hat{\mathbf{K}})$ frame. $(\hat{\mathbf{a}}, \hat{\mathbf{b}}, \hat{\mathbf{c}})$ is denoted as $(\vec{P}, \vec{Q}, \vec{k})$ in [13].

Coordinate systems. The tensorial background $\bar{s}^{\mu\nu}$ is *observer* LI, while *particle* LV. Therefore, to probe the magnitudes of $\bar{s}^{\mu\nu}$, one should explicitly point out the observer coordinate system in use. In the context of post-Newtonian gravity of SME, the standard frame is an asymptotically inertial frame, $(\mathrm{T}, \hat{\mathbf{X}}, \hat{\mathbf{Y}}, \hat{\mathbf{Z}})$, that is comoving with the Solar system [13] (see Fig. 1). For a pulsar binary, the most convenient frame, $(t, \hat{\mathbf{a}}, \hat{\mathbf{b}}, \hat{\mathbf{c}})$, is defined by the orbit (see Fig. 2). To relate two frames, in general a Lorentz transformation is required [13]. It consists of a spatial rotation, $\mathcal{R}$, to align $(\hat{\mathbf{a}}, \hat{\mathbf{b}}, \hat{\mathbf{c}})$ and $(\hat{\mathbf{X}}, \hat{\mathbf{Y}}, \hat{\mathbf{Z}})$, and a boost characterized by the relative velocity of the pulsar system with respect to the Solar system. Typically, its magnitude equals to $\mathcal{O}(10^2\,\mathrm{km/s})$, which implies a boost of $\mathcal{O}(10^{-3})$ that is neglected here. We are left with a pure spatial rotation $\mathcal{R}$. It can be obtained with the help of an intermediate coordinate system, $(\hat{\mathbf{I}}, \hat{\mathbf{J}}, \hat{\mathbf{K}})$ (see Figs. 1–2). It involves five simple steps to transform from $(\hat{\mathbf{a}}, \hat{\mathbf{b}}, \hat{\mathbf{c}})$ to $(\hat{\mathbf{X}}, \hat{\mathbf{Y}}, \hat{\mathbf{Z}})$, characterized by α (right ascension), δ (declination), Ω (longitude of ascending node), i (orbital inclination), and ω (longitude of periastron). The full rotation $\mathcal{R} = \mathcal{R}^{(\omega)}\mathcal{R}^{(i)}\mathcal{R}^{(\Omega)}\mathcal{R}^{(\delta)}\mathcal{R}^{(\alpha)}$ [26]. The transformations of $\bar{s}^{\mu\nu}$ are $\bar{s}^{tt} \doteq \bar{s}^{\mathrm{TT}}$, $\bar{s}^{AB} \doteq \mathcal{R}^{A}_{\ x}\mathcal{R}^{B}_{\ y}\bar{s}^{xy}$, and $\bar{s}^{tA} \doteq \mathcal{R}^{A}_{\ x}\bar{s}^{\mathrm{T}x}$, where $A, B = a, b, c$ and $x, y = \mathrm{X}, \mathrm{Y}, \mathrm{Z}$.

Spin precession of solitary pulsars. Following the derivations in [27], one gets an extra precession, $\mathbf{\Omega}^{\mathrm{prec}}$, for an isolated spinning body in internal equilibrium [13]. The precession rate is $\Omega_k^{\mathrm{prec}} = \pi \bar{s}^{jk}\hat{S}^j/P$, where P is the spin period, and $\hat{\mathbf{S}}$ is the unit vector pointing along the spin direction. Because of their small spin periods, millisecond pulsars (MSPs) are ideal objects to probe such a precession [27, 28]. We follow the methodology in [28] to relate the precession with observables in pulse profile. The precession will manifest itself in terms of a change in the angle λ, which is defined to be the angle between $\hat{\mathbf{K}}$ and $\hat{\mathbf{S}}$ (see Fig. 2). Purely from geometry one has, $\dot{\lambda} = \hat{\mathbf{e}} \cdot \mathbf{\Omega}^{\mathrm{prec}} = \pi \bar{s}^{jk}\hat{S}^j\hat{e}^k/P$ [28], where the unit vector $\hat{\mathbf{e}} \equiv \hat{\mathbf{K}} \times \hat{\mathbf{S}}/|\hat{\mathbf{K}} \times \hat{\mathbf{S}}|$ gives the line of nodes associated with the intersection of the equatorial plane of the pulsar and the sky plane. Further, we introduce a simple pulsar emission model, the cone model [29], to relate the change in λ with the change in pulse width. Details can be found in [26, 28]. Notice that $\hat{\mathbf{e}} \perp \hat{\mathbf{S}}$ by definition, therefore we are insensitive to $\bar{s}^{\mathrm{TT}} = \bar{s}^{\mathrm{XX}} + \bar{s}^{\mathrm{YY}} + \bar{s}^{\mathrm{ZZ}}$ with solitary pulsars.

Orbital dynamics of binary pulsars. In presence of LV effects, the orbital dynamics of a binary is modified [13]. By using the technique of osculating elements, Bailey and Kostelecký calculated secular changes for orbital elements [13, 26]. We here give an equivalent, but more compact, vectorial form for $\mathbf{e} \equiv e\hat{\mathbf{a}}$ and $\mathbf{l} \equiv \sqrt{1-e^2}\hat{\mathbf{c}}$ [30, 31] after averaging over an orbit,

$$\begin{aligned}\left\langle \frac{\mathrm{d}\mathbf{e}}{\mathrm{d}t} \right\rangle &= e\dot{\omega}_{\mathrm{R}}\hat{\mathbf{b}} \\ &-n_b e F_e \left(F_e\sqrt{1-e^2}\bar{s}^{ab}\hat{\mathbf{a}} - F_e\frac{\bar{s}^{aa}-\bar{s}^{bb}}{2}\hat{\mathbf{b}} + \bar{s}^{bc}\hat{\mathbf{c}} \right) \\ &+2\delta X\,\mathcal{V}_{\mathrm{O}} n_b F_e \left(\sqrt{1-e^2}\bar{s}^{0a}\hat{\mathbf{a}} + \bar{s}^{0b}\hat{\mathbf{b}} - \frac{e^2}{\sqrt{1-e^2}}\bar{s}^{0c}\hat{\mathbf{c}} \right) , \end{aligned} \tag{2}$$

$$\begin{aligned}\left\langle \frac{\mathrm{d}\mathbf{l}}{\mathrm{d}t} \right\rangle &= n_b F_e \left(\sqrt{1-e^2}\bar{s}^{bc}\hat{\mathbf{a}} - \bar{s}^{ac}\hat{\mathbf{b}} + e^2 F_e \bar{s}^{ab}\hat{\mathbf{c}} \right) \\ &+2\delta X\,\mathcal{V}_{\mathrm{O}} n_b e F_e \left(\bar{s}^{0c}\hat{\mathbf{a}} - \bar{s}^{0a}\hat{\mathbf{c}} \right) , \end{aligned} \tag{3}$$

TABLE I. Pulsar constraints on the coefficients of the pure-gravity sector of mSME [13]. The K-factor reflects the improvement over the combined limits from LLR and AI [24]. Notice the probabilistic assumption made in the text.

SME coefficients	68% confidence level	K-factor
$\bar{s}^{\rm TX}$	$(-5.2,\ 5.3)\times10^{-9}$	118
$\bar{s}^{\rm TY}$	$(-7.5,\ 8.5)\times10^{-9}$	163
$\bar{s}^{\rm TZ}$	$(-5.9,\ 5.8)\times10^{-9}$	650
$\bar{s}^{\rm XY}$	$(-3.5,\ 3.6)\times10^{-11}$	42
$\bar{s}^{\rm XZ}$	$(-2.0,\ 2.0)\times10^{-11}$	70
$\bar{s}^{\rm YZ}$	$(-3.3,\ 3.3)\times10^{-11}$	42
$\bar{s}^{\rm XX}-\bar{s}^{\rm YY}$	$(-9.7,\ 10.1)\times10^{-11}$	16
$\bar{s}^{\rm XX}+\bar{s}^{\rm YY}-2\bar{s}^{\rm ZZ}$	$(-12.3,\ 12.2)\times10^{-11}$	310

where $\dot{\omega}_{\rm R}$ is the periastron advance rate, $n_b\equiv 2\pi/P_b$ is the orbital frequency, $\mathcal{V}_{\rm O}\equiv[G(m_1+m_2)n_b]^{1/3}$ is the characteristic orbital velocity, and $\delta X\equiv\frac{m_1-m_2}{m_1+m_2}$ denotes the difference of the pulsar mass m_1 and the companion mass m_2. The function $F_e\equiv\frac{1}{1+\sqrt{1-e^2}}$ only depends on the eccentricity e, and $F_e\in[\frac{1}{2},1)$ for a bound orbit.

In pulsar timing, in principle one can construct three tests per binary to constrain LV effects, by utilizing $\dot{\omega}$, $\dot{e}$, and $\dot{x}$ (x is the projected semimajor axis of pulsar orbit) [13, 26]. Through a direct check, one can show that they are insensitive to $\bar{s}^{\rm TT}$ as well.

Simulations and results. Thirteen pulsars are chosen for tests, including profile observations of two solitary MSPs, PSRs B1937+21 and J1744−1134 [28], that provide one test per pulsar, and timing observations of eleven binaries, PSRs B1913+16 [32], B1534+12 [33], J0737−3039A [34], B2127+11C [35], J1738+0333 [36], J1012+5307 [37], J0348+0432 [38], J1802−2124 [39], J0437−4715 [40], B1855+09, and J1909−3744 [41], that provide two or three tests per system. In total we constructed twenty-seven tests [26].

Specifically, the null detection of any change in the morphology of the pulse profiles of two solitary pulsars, after being monitored for more than one decade [28], tightly constrains the LV spin precession. For binary pulsars, we use the published timing solutions of the successful phase-coherent fittings to times of arrival of pulse signals with generic timing models [32–41]. The observations extend several years to decades. The null detection of any beyong-GR effects in binary pulsars constrains LV orbital dynamics. All these pulsar systems were studied in great details in their original publications, and relevant results are reviewed and discussed in [26].

We made following considerations in our calculation. i) Because usually $\dot{x}$ and $\dot{e}$ were not reported in literature, we conservatively estimate 68% CL upper limits for them from uncertainties of e and x, as $|\dot{e}|^{\rm upper}=\sqrt{12}\sigma_e/T_{\rm obs}$ and $|\dot{x}|^{\rm upper}=\sqrt{12}\sigma_x/T_{\rm obs}$ [26], where $T_{\rm obs}$ is the time span used in deriving the timing solution, in accordence with the case of linear-in-time evolution. The estimation is consistent with the values reported in [33] for PSR B1534+12. We also account for the contribution to $\dot{x}$ from proper motion [42]. ii) For consistency, the $\dot{\omega}$ test is possible only if component masses are measured to a high precision independent of gravity theories. Such mass measurements are possible only with a few small-eccentricity binary pulsars with optical observations of companions [36–38]. Because these binaries have no $\dot{\omega}$ measurements yet, we use the limits on time variations of the eccentricity vector in tests with an $\dot{\omega}$ calculted from GR, similar to the method proposed in [31]. We don't use $\dot{\omega}$ in tests for pulsars whose masses were based on GR. In contrast, $\dot{e}$ and $\dot{x}$ tests are still feasible with them because in GR the changes in x and e introduced by gravitational damping are negligible [29], hence only modest knowledge on component masses is sufficient. iii) One caution in directly using Eqs. (2–3) was pointed out in [43] that a large $\dot{\omega}$ can render the secular changes nonconstant. These effects cannot be too large based on the fact that all binaries were well fitted with simple timing models. The largest change in ω is $\sim100^\circ$ for PSR B1913+16 in our samples. Therefore, we consider it safe to use time-averaged values for ω-related quantities as a rough approximation at current stage. vi) The geometry of above pulsar systems is not fully determined from observations. For binary pulsars, the longitude of ascending node, Ω, is generally not an observable in pulsar timing, while for solitary pulsars, the azimuthal angle of the spin, η, is unknown. We have to treat them as random variables uniformly distributed in $[0^\circ,360^\circ)$. This choice makes our tests as probabilistic tests.

We set up Monte Carlo simulations to treat unknown angles and measurement uncertainties. First, we make lots of trials to identify the eight most stringent tests. Linear equations for LV coefficients are constructed from them. The equation set is solved to obtain eight combinations of LV coefficients. Afterwards we check whether these values are also consistent with the other nineteen tests. If all tests are passed, values are stored. We accumulate 10^4 entries and read out the 68% CLs for LV coefficients. Results are tabulated in Table I, where a comparison with that from the combination of Lunar Laser Ranging (LLR) and atom interferometry (AI) [24] is made. The *improvement factor*, K, is defined to be the (inverse) ratio of the length of 68% CLs. In Fig. 3, 10^3 entries out of our results are plotted. The absence of obvious correltaions between different coefficients benefits from multiple pulsars which make unlikely for a specific combination of large LV coefficients to pass *all* tests.

Discussions. In the parametrized post-Newtonian (PPN) formalism, there are two parameters, α_1 and α_2, together with an absolute velocity with repsect to a preferred frame, $\mathbf{w}$, to describe semiconservative LV effects [1, 2]. We notice that if we do the replacements in the pure-gravity sector of mSME, $\bar{s}^{0j}\to\alpha_1 w^j/4$ and

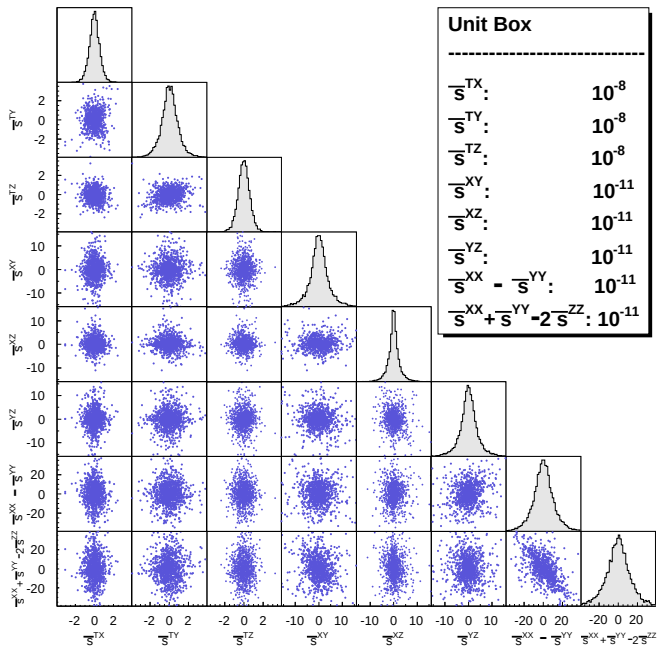

FIG. 3. Correlations of LV coefficients and marginalized probability densities. Only 10^3 points out of 10^4 simulations are plotted in each panel for clearity.

$\bar{s}^{jk} \to -\alpha_2 w^j w^k$, the dynamics of PPN is exactly recovered. We can clearly see the relation from Lagrangians or from a comparison between Eqs. (2–3) and Eqs. (13–19) in [31]. This new relation was also discussed by Bailey and Kostelecký in a different manner, see Eq. (68) in [13].

In scalar-tensor theories, strong fields associated with neutron stars may develop nonperturbative effects [44]. One would expect similar effects in SME. Therefore our results in Table I are, strictly speaking, *effective* constraints that include strong-field contributions.

The tests here are of probabilistic nature because of unknown angles Ω and η. High-precision timing of nearby pulsars (e.g. PSR J0437−4715 [40]) and observations of interstellar scintillation (e.g. PSR B1534+12 [45]) may determine Ω. When more such measurements are available, robust tests can be performed.

All tests in this Letter are based on time derivatives of observables, whose precisions improve as $T_{\rm obs}^{-3/2}$. Continuous observations can quickly improve all tests. Especially in the era of FAST and SKA telescopes, more pulsars and high sensitivities will further enable better tests of gravity. We also notice that some timing results used here were reported more than one decade ago. New results for sure have already improved a lot. We hope observers report $\dot{e}$ and $\dot{x}$ measurements whenever feasible, which can give more realistic constraints for LV coefficients. It is also possible to use dissipative effects [46] once gravitational radiation is calculated in SME.

Recently, Bailey et al. [47] obtained the first constraint of the $\bar{s}^{\rm TT} = \bar{s}^{\rm XX} + \bar{s}^{\rm YY} + \bar{s}^{\rm ZZ}$ component from Gravity Probe B. Their result $|\bar{s}^{\rm TT}| < 3.8\times10^{-3}$ (68% CL) can be combined with ours to break all degeneracy. We also note that the boost between a pulsar system and the Solar system can be used to mix $\bar{s}^{\rm TT}$ with other components, hence provides the possibility to obtain a constraint of $\bar{s}^{\rm TT}$ directly from pulsars. Currently, only a few pulsars with optical observations of their companions have 3 D velocity measurements that are needed for the boost calculation. We expect more measurements will achieve the goal in the future.

We thank Norbert Wex for stimulating discussions and carefully reading the manuscript. We are grateful to Jay Tasson for encouragements, Joris Verbiest for discussions, and three anonymous referees for comments. Lijing Shao is supported by China Scholarship Council (CSC).

* lshao@pku.edu.cn

[1] C. M. Will, *Theory and Experiment in Gravitational Physics* (Cambridge University Press, 1993).
[2] C. M. Will, Living Rev. Rel. **9**, 3 (2006).
[3] V. A. Kostelecký and S. Samuel, Phys. Rev. D **39**, 683 (1989).
[4] V. A. Kostelecký and S. Samuel, Phys. Rev. D **40**, 1886 (1989).
[5] D. Colladay and V. A. Kostelecký, Phys. Rev. D **55**, 6760 (1997).
[6] D. Colladay and V. A. Kostelecký, Phys. Rev. D **58**, 116002 (1998).
[7] R. Gambini and J. Pullin, Phys. Rev. D **59**, 124021 (1999).
[8] T. Jacobson and D. Mattingly, Phys. Rev. D **64**, 024028 (2001).
[9] F. R. Klinkhamer, Nucl. Phys. B **578**, 277 (2000).
[10] V. A. Kostelecký and M. Mewes, Phys. Rev. D **66**, 056005 (2002).
[11] V. A. Kostelecký, Phys. Rev. D **69**, 105009 (2004).
[12] R. Bluhm and V. A. Kostelecký, Phys. Rev. D **71**, 065008 (2005).
[13] Q. G. Bailey and V. A. Kostelecký, Phys. Rev. D **74**, 045001 (2006).
[14] P. Hořava, Phys. Rev. D **79**, 084008 (2009).
[15] V. A. Kostelecký and J. D. Tasson, Phys. Rev. D **83**, 016013 (2011).
[16] V. A. Kostelecký and N. Russell, Rev. Mod. Phys. **83**, 11 (2011).
[17] G. Amelino-Camelia, Living Rev. Rel. **16**, 5 (2013).
[18] S. Liberati, Class. Quantum Grav. **30**, 133001 (2013).
[19] O. Nachtmann, Conf. Proc. C **690224**, 485 (1969).
[20] S. Chadha and H. B. Nielsen, Nucl. Phys. B **217**, 125 (1983).
[21] S. Weinberg, PoS CD **09**, 001 (2009).
[22] J. B. R. Battat, J. F. Chandler, and C. W. Stubbs, Phys. Rev. Lett. **99**, 241103 (2007).
[23] H. Müller, S.-W. Chiow, S. Herrmann, S. Chu, and K.-Y. Chung, Phys. Rev. Lett. **100**, 031101 (2008).
[24] K.-Y. Chung, S.-W. Chiow, S. Herrmann, S. Chu, and

H. Müller, Phys. Rev. D **80**, 016002 (2009).
[25] T. Damour and J. H. Taylor, Phys. Rev. D **45**, 1840 (1992).
[26] Supplemental material.
[27] K. Nordtvedt, Astrophys. J. **320**, 871 (1987).
[28] L. Shao, R. N. Caballero, M. Kramer, et al., Class. Quantum Grav. **30**, 165019 (2013).
[29] D. R. Lorimer and M. Kramer, *Handbook of Pulsar Astronomy*, (Cambridge University Press, 2005).
[30] T. Damour and G. Esposito-Farèse, Phys. Rev. D **46**, 4128 (1992).
[31] L. Shao and N. Wex, Class. Quantum Grav. **29**, 215018 (2012).
[32] J. M. Weisberg, D. J. Nice, and J. H. Taylor, ApJ **722**, 1030 (2010).
[33] I. H. Stairs, S. E. Thorsett, J. H. Taylor, and A. Wolszczan, Astrophys. J. **581**, 501 (2002).
[34] M. Kramer, I. H. Stairs, R. N. Manchester, et al., Science **314**, 97 (2006).
[35] B. A. Jacoby, P. B. Cameron, F. A. Jenet, et al., ApJL **644**, L113 (2006).
[36] P. C. C. Freire, N. Wex, G. Esposito-Farèse, et al., MNRAS **423**, 3328 (2012).
[37] K. Lazaridis, N. Wex, A. Jessner, et al., MNRAS **400**, 805 (2009).
[38] J. Antoniadis, P. C. C. Freire, N. Wex, et al., Science **340**, 448 (2013).
[39] R. D. Ferdman, I. H. Stairs, M. Kramer, et al., ApJ **711**, 764 (2010).
[40] J. P. W. Verbiest, M. Bailes, W. van Straten, et al., ApJ **679**, 675 (2008).
[41] J. P. W. Verbiest, M. Bailes, W. A. Coles, et al., MNRAS **400**, 951 (2009).
[42] S. M. Kopeikin, ApJ **467**, L93 (1996).
[43] N. Wex and M. Kramer, MNRAS **380**, 455 (2007).
[44] T. Damour and G. Esposito-Farèse, Phys. Rev. Lett. **70**, 2220 (1993).
[45] S. Bogdanov, M. Pruszyńska, W. Lewandowski, and A. Wolszczan, Astrophys. J. **581**, 495 (2002).
[46] K. Yagi, D. Blas, E. Barausse, and N. Yunes, arXiv:1311.7144.
[47] Q. G. Bailey, R. D. Everett, and J. M. Overduin, Phys. Rev. D**88**, 102001 (2013).

Supplemental Material

Lijing Shao (MPIfR & PKU)

ROTATION MATRICES

The transformation matrix $\mathcal{R}$ from the Sun-centered celestial-equatorial coordinate system, $(\hat{\mathbf{X}}, \hat{\mathbf{Y}}, \hat{\mathbf{Z}})$, to the binary coordinate system, $(\hat{\mathbf{a}}, \hat{\mathbf{b}}, \hat{\mathbf{c}})$, can be decomposed into five simple parts,

$$\begin{pmatrix} \hat{\mathbf{a}} \\ \hat{\mathbf{b}} \\ \hat{\mathbf{c}} \end{pmatrix} = \mathcal{R} \begin{pmatrix} \hat{\mathbf{X}} \\ \hat{\mathbf{Y}} \\ \hat{\mathbf{Z}} \end{pmatrix} , \tag{1}$$

with

$$\mathcal{R} = \mathcal{R}^{(\omega)}\mathcal{R}^{(i)}\mathcal{R}^{(\Omega)}\mathcal{R}^{(\delta)}\mathcal{R}^{(\alpha)} . \tag{2}$$

For a binary pulsar, explicit expressions of these matrices are

$$\mathcal{R}^{(\alpha)} = \begin{pmatrix} -\sin\alpha & \cos\alpha & 0 \\ -\cos\alpha & -\sin\alpha & 0 \\ 0 & 0 & 1 \end{pmatrix} , \tag{3}$$

$$\mathcal{R}^{(\delta)} = \begin{pmatrix} 1 & 0 & 0 \\ 0 & \sin\delta & \cos\delta \\ 0 & -\cos\delta & \sin\delta \end{pmatrix} , \tag{4}$$

$$\mathcal{R}^{(\Omega)} = \begin{pmatrix} \cos\Omega & \sin\Omega & 0 \\ -\sin\Omega & \cos\Omega & 0 \\ 0 & 0 & 1 \end{pmatrix} , \tag{5}$$

$$\mathcal{R}^{(i)} = \begin{pmatrix} 1 & 0 & 0 \\ 0 & \cos i & \sin i \\ 0 & -\sin i & \cos i \end{pmatrix} , \tag{6}$$

$$\mathcal{R}^{(\omega)} = \begin{pmatrix} \cos\omega & \sin\omega & 0 \\ -\sin\omega & \cos\omega & 0 \\ 0 & 0 & 1 \end{pmatrix} , \tag{7}$$

where α (right ascension), δ (declination), Ω (longitude of ascending node), i (orbital inclination), ω (longitude of periastron) are defined in Figs. 1–2 in the main text.

For a solitary pulsar, only a rotation from $(\hat{\mathbf{X}}, \hat{\mathbf{Y}}, \hat{\mathbf{Z}})$ to $(\hat{\mathbf{I}}, \hat{\mathbf{J}}, \hat{\mathbf{K}})$ is needed, hence one can set $\mathcal{R}^{(\Omega)}$, $\mathcal{R}^{(i)}$, and $\mathcal{R}^{(\omega)}$ to unit matrices.

PULSAR EMISSION MODEL AND LV SPIN PRECESSION

As in [28], we adopt the cone model for pulsar emission [29]. Other choices only affect the results marginally. In the cone model, from the geometry, one has,

$$\sin^2\left(\frac{W}{4}\right) = \frac{\sin^2(\rho/2) - \sin^2(\beta/2)}{\sin(\alpha+\beta)\sin\alpha} , \tag{8}$$

where W is the width of the pulse, α is the magnetic inclination angle, $\beta \equiv 180^\circ - \lambda - \alpha$ is the impact angle, and ρ is the semi-angle of the opening radiating region. Adopting a plausible assumption that the radiation property has no change during the observational span, i.e. $\mathrm{d}\alpha/\mathrm{d}t = \mathrm{d}\rho/\mathrm{d}t = 0$, one has [28],

$$\frac{\mathrm{d}\lambda}{\mathrm{d}t} = \frac{1}{2}\frac{\sin(W/2)}{\cot\lambda\cos(W/2) + \cot\alpha}\frac{\mathrm{d}W}{\mathrm{d}t} . \tag{9}$$

Combining it with the LV spin precession rate, $\Omega_k^{\rm prec} = \pi\bar{s}^{jk}\hat{S}^j/P$, and the geometric relation, $\dot{\lambda} = \hat{\mathbf{e}}\cdot\boldsymbol{\Omega}^{\rm prec}$ (see the main text), one can relate the LV coefficients with the time derivative of the pulse width,

$$\frac{\mathrm{d}W}{\mathrm{d}t} = \frac{2\pi}{P}\frac{\cot\lambda\cos(W/2) + \cot\alpha}{\sin(W/2)}\bar{s}^{jk}\hat{S}^j\hat{e}^k . \tag{10}$$

ORBITAL DYNAMICS OF A BINARY IN PRESENCE OF LV EFFECTS

We collect from [13] with slightly different notations the orbital-averaged secular changes of a, e, ω, and x,

$$\left\langle\frac{\mathrm{d}a}{\mathrm{d}t}\right\rangle = 0 , \tag{11}$$

$$\left\langle\frac{\mathrm{d}e}{\mathrm{d}t}\right\rangle = n_b F_e\sqrt{1-e^2}\left(-eF_e\bar{s}^{ab} + 2\delta X\,\mathcal{V}_{\rm O}\bar{s}^{0a}\right) , \tag{12}$$

$$\begin{aligned}\left\langle\frac{\mathrm{d}\omega}{\mathrm{d}t}\right\rangle = {}& \frac{3n_b\mathcal{V}_{\rm O}^2}{1-e^2} - \frac{n_b F_e\cot i}{\sqrt{1-e^2}}\times \\ & \left(\sin\omega\,\bar{s}^{ac} + \sqrt{1-e^2}\cos\omega\,\bar{s}^{bc} + 2\delta X\,e\mathcal{V}_{\rm O}\cos\omega\,\bar{s}^{0c}\right) \\ & + n_b F_e\left(F_e\frac{\bar{s}^{aa}-\bar{s}^{bb}}{2} + \frac{2}{e}\delta X\,\mathcal{V}_{\rm O}\bar{s}^{0b}\right) ,\end{aligned} \tag{13}$$

$$\begin{aligned}\left\langle\frac{\mathrm{d}x}{\mathrm{d}t}\right\rangle = {}& \frac{1-\delta X}{2}\frac{F_e\mathcal{V}_{\rm O}\cos i}{\sqrt{1-e^2}}\times \\ & \left(\cos\omega\,\bar{s}^{ac} - \sqrt{1-e^2}\sin\omega\,\bar{s}^{bc} - 2\delta X\,e\mathcal{V}_{\rm O}\sin\omega\,\bar{s}^{0c}\right) ,\end{aligned} \tag{14}$$

where a is the semimajor axis of the *orbit* and x is the projected semimajor axis of the *pulsar*. Other notations are given in the main text. These equations are equivalent to Eqs. (2–3) in the main text.

In the limit of small eccentricity ($e \ll 1$), above equations reduce to

$$\left\langle\frac{\mathrm{d}a}{\mathrm{d}t}\right\rangle = 0 , \tag{15}$$

$$\left\langle\frac{\mathrm{d}e}{\mathrm{d}t}\right\rangle \simeq n_b\delta X\,\mathcal{V}_{\rm O}\bar{s}^{0a} , \tag{16}$$

$$\left\langle\frac{\mathrm{d}\omega}{\mathrm{d}t}\right\rangle \simeq 3n_b\mathcal{V}_{\rm O}^2 + \frac{n_b}{e}\delta X\,\mathcal{V}_{\rm O}\bar{s}^{0b} , \tag{17}$$

$$\left\langle\frac{\mathrm{d}x}{\mathrm{d}t}\right\rangle \simeq \frac{1-\delta X}{4}\mathcal{V}_{\rm O}\cos i\left(\bar{s}^{ac}\cos\omega - \bar{s}^{bc}\sin\omega\right) . \tag{18}$$

Time derivatives of two Laplace-Lagrange parameters are easily obtained from Eqs. (15–18),

$$\left\langle \frac{\mathrm{d}\eta}{\mathrm{d}t} \right\rangle \simeq n_b \delta X \mathcal{V}_{\rm O} \left(\bar{s}^{0a} \sin\omega + \bar{s}^{0b} \cos\omega \right) + 3 e n_b \mathcal{V}_{\rm O}^2 \cos\omega \quad (19)$$

$$\left\langle \frac{\mathrm{d}\kappa}{\mathrm{d}t} \right\rangle \simeq n_b \delta X \mathcal{V}_{\rm O} \left(\bar{s}^{0a} \cos\omega - \bar{s}^{0b} \sin\omega \right) - 3 e n_b \mathcal{V}_{\rm O}^2 \sin\omega \quad (20)$$

where $\eta \equiv e\sin\omega$ and $\kappa \equiv e\cos\omega$.

A BRIEF OVERVIEW OF PULSAR SYSTEMS USED IN LV TESTS

In testing the pure-gravity sector of mSME, 13 pulsar systems are used. The binaries are selected mainly based on their orbital compactness and timing precision. From equations above, it is easy to see that binary pulsars with short orbital periods are perferred to perform LV tests. The distribution of our pulsars in the sky is plotted in Fig. 4. The wide coverage with multiple pulsar systems, in terms of positional direction and orbital geometry, helps to disentangle the degeneracy of LV coefficients [13].

Relevant parameters of our pulsar systems for LV tests are tabulated in Tables I–IV. We have grouped them into solitary pulsars (PSRs B1937+21 and J1744−1134 [28]; Table I), small-eccentricity binary pulsars with theory-independent mass measurements (PSRs J1012+5307 [37], J1738+0333 [36], and J0348+0432 [38]; Table II), small-eccentricity binary pulsars without theory-independent mass measurements (PSRs J1802−2124 [39], J0437−4715 [40], B1855+09, and J1909−3744 [41]; Table III), and eccentric binary pulsars (PSRs B1913+16 [32], B1534+12 [33], B2127+11C [35], and J0737−3039A [34]; Table IV). Brief reviews of each pulsar system are given below, and interested readers are pointed to original publications and references therein for details.

By using the phrase "*pulsars with theory-independent mass measurements*", we refer to those binary pulsars that have mass measurements only based on the weak-field gravity theory, whose validity has already been well-tested in the Solar system [2]. In our samples, three small-eccentricity binary pulsars have such mass measurements [36–38]. The optical observations of their white dwarf (WD) companions give the masses of WDs from well-established WD models. Combining the optical and radio observations, one can obtain the mass ratio, $q \equiv m_1/m_2$, from the amplitudes of their projected orbital velocities along the line of sight. In contrast, "*pulsars without theory-independent mass measurements*" refer to binary pulsars that have masses derived from post-Newtonian effects of GR. If these effects with strongly self-gravitating bodies were modified in alternative gravity theories, the GR masses cannot be trusted with high confidence in precision tests of alternative gravity theories. For the reasons stated in the main text, we can use component masses derived from GR as an approximation in $\dot{e}$ and $\dot{x}$ tests.

In our LV tests, solitary pulsars provide one test per system with Eq. (10), and binary pulsars with theory-independent mass measurements provide three tests per system with Eq. (18) and the time variations of the eccentricity vector[1], while bianry pulsars without theory-independent mass measurements provide two tests per system with Eqs. (12) and (14). Therefore, in total, we have performed 27 tests on 8 linear combinations of LV coefficients.

Solitary pulsars

PSR B1937+21

PSR B1937+21 (a.k.a. PSR J1939+2134) is the first discovered MSP, with a spin period of 1.56 ms. It is a bright pulsar in the radio band and has a stable rotation. Therefore, PSR B1937+21 was chosen as an important target in the pulsar timing array (PTA) projects, and has been observed continuously and frequently since its discovery in 1982. Although with substantial low-frequency red noises, the timing residual has reached a level $\lesssim 0.4\,\mu$s [41]. Recently, Shao et al. [28] analyzed ~ 15 years of archival data, taken at the 100-m Effelsberg radio telescope, to look into the stability of the pulse profile of this pulsar. The profile consists of a main-pulse and an interpulse. They are both very stable with their time derivatives of width constrained to be $(-3.2\pm3.4)\times10^{-3}\,\mathrm{deg\,yr^{-1}}$ and $(3.5\pm6.6)\times10^{-3}\,\mathrm{deg\,yr^{-1}}$ respectively [28]. The null change in pulse width indicates a null LV spin precession.

PSR J1744−1134

PSR J1744−1134 was discovered in 1997 through the Parkes 436 MHz survey of the southern sky. The pulsar has a spin period of 4.07 ms, and later was chosen as a target in PTA projects, being observed frequently as well. The timing residual reaches sub-μs in [41]. This pulsar has a clear main-pulse, and the pulse profile is very stable against time, whose time derivative of the pulse width was constrained to be $(1.3\pm7.2)\times10^{-3}\,\mathrm{deg\,yr^{-1}}$ from 15 years of Effelsberg data [28].

[1] With the new relation between the pure-gravity sector of mSME and the PPN framework in the main text, it is easy to check that for small-eccentricity binary pulsars, the time-spatial components of $\bar{s}^{\mu\nu}$ introduce "*orbital polarization effects*", in a similar way to that introduced by the PPN parameter α_1 [31]. This can also be easily checked from Eqs. (16) and (17).

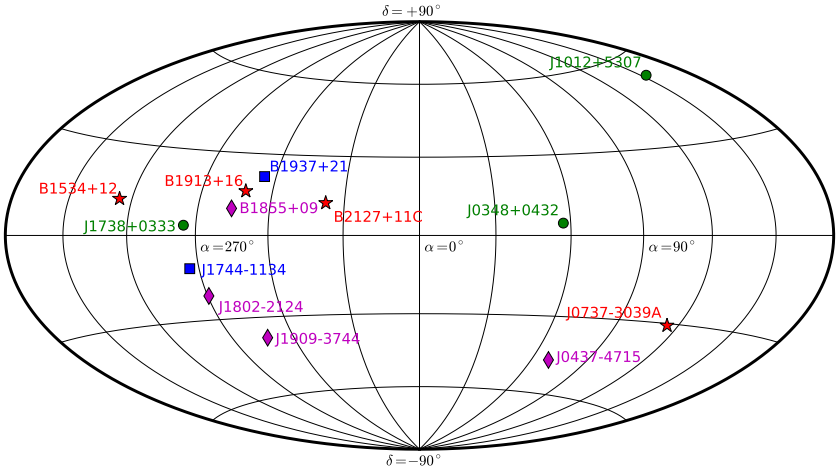

FIG. 4. Distributions of pulsar systems in the sky used in tests of the pure-gravity sector of mSME. Blue squares, green circles, magenta diamonds, and red stars denote solitary pulsars, small-eccentricity binary pulsars with theory-independent mass measurements, small-eccentricity binary pulsars without theory-independent mass measurements, and eccentric binary pulsars, respectively.

TABLE I. Relevant quantities of PSRs B1937+21 and J1744−1134 for the test. Most quantities are from pulsar timing, while the orientation and radiation quantities (α and ζ) were obtained from the model fitting to radio and γ-ray lightcurves (see [28] and references therein). For PSR B1937+21, quantities for the main-pulse (left) and the interpulse (right) are both tabulated. Parenthesized numbers represent the 1-σ uncertainty in the last digits quoted.

Pulsar	PSR B1937+21	PSR J1744−1134
Discovery (year)	1982	1997
Right Ascension, α (J2000)	$19^{\rm h}39^{\rm m}38^{\rm s}.561297(2)$	$17^{\rm h}44^{\rm m}29^{\rm s}.403209(4)$
Declination, δ (J2000)	$+21^\circ34'59''.12950(4)$	$-11^\circ34'54''.6606(2)$
Spin period, P (ms)	1.55780653910(3)	4.074545940854022(8)
Proper motion in α, μ_α (mas yr^{-1})	0.072(1)	18.804(8)
Proper motion in δ, μ_δ (mas yr^{-1})	−0.415(2)	−9.40(3)
Magnetic inclination, α (deg)	75^{+8}_{-6} / 105^{+6}_{-8}	51^{+16}_{-19}
Observer angle, $\zeta \equiv 180^\circ - \lambda$ (deg)	80(3)	85^{+3}_{-12}
Time span of data (MJD)	50693–55725	50460–55962
Pulse width at 50% intensity, W_{50} (deg)	8.281(9) / 10.245(17)	12.53(3)
Time derivative of W_{50}, dW_{50}/dt (10^{-3} deg yr^{-1})	−3.2(34) / 3.5(66)	1.3(72)

Small-eccentricity binary pulsars with theory-independent mass measurements

PSR J1012+5307

PSR J1012+5307 is a small-eccentricity neutron star (NS) white dwarf (WD) binary system, with an orbital period of 14.5 hours. The pulsar was discovered in 1993 with the 76-m Lovell radio telescope at Jodrell Bank. Later optical observations revealed its companion being a helium WD, and determined the mass ratio $q \equiv m_1/m_2 = 10.5 \pm 0.5$, and the WD mass $m_2 = 0.16 \pm 0.02\,{\rm M}_\odot$. The 3 D spatial velocity of this binary was also measured. Lazaridis et al. [37] presented the most updated timing solution by using 15 years of observations from the European PTA (EPTA) network, from which they obtained stringent limits on the gravitational dipole radiation and the time variation of the gravitational constant. Being a well-timed relativistic binary, PSR J1012+5307 is useful to constrain local Lorentz invariance violation of gravity. It was used to constrain the PPN parameters, α_1 and α_2, in tests proposed in [31].

TABLE II. Relevant quantities of PSRs J1012+5307 [37], J1738+0333 [36], and J0348+0432 [38] for the test, from radio-timing and optical observations. Parenthesized numbers represent the 1-σ uncertainty in the last digits quoted. The listed Laplace-Lagrange parameter, η, is the intrinsic value, after subtraction of the contribution from the Shapiro delay. There is an ambiguity between i and $180^\circ - i$; only the value $i < 90^\circ$ is tabulated.

Pulsar	PSR J1012+5307	PSR J1738+0333	PSR J0348+0432
`Observed Quantities`			
Observational span, $T_{\rm obs}$ (year)	~ 15 [37]	~ 10 [36]	~ 4 [38]
Right ascension, α (J2000)	$10^{\rm h}12^{\rm m}33\overset{\rm s}{.}4341010(99)$	$17^{\rm h}38^{\rm m}53\overset{\rm s}{.}9658386(7)$	$03^{\rm h}48^{\rm m}43\overset{\rm s}{.}639000(4)$
Declination, δ (J2000)	$53^\circ07'02''.60070(13)$	$03^\circ33'10''.86667(3)$	$04^\circ32'11''.4580(2)$
Proper motion in α, μ_α (mas yr^{-1})	2.562(14)	7.037(5)	4.04(16)
Proper motion in δ, μ_δ (mas yr^{-1})	$-25.61(2)$	5.073(12)	3.5(6)
Spin period, P (ms)	5.255749014115410(15)	5.850095859775683(5)	39.1226569017806(5)
Orbital period, $P_{\rm b}$ (day)	0.60467271355(3)	0.3547907398724(13)	0.102424062722(7)
Projected semimajor axis, x (lt-s)	0.5818172(2)	0.343429130(17)	0.14097938(7)
$\eta \equiv e\sin\omega$ (10^{-7})	-1.4 ± 3.4	-1.4 ± 1.1	19 ± 10
$\kappa \equiv e\cos\omega$ (10^{-7})	0.6 ± 3.1	3.1 ± 1.1	14 ± 10
Time derivative of x, $\dot{x}$ (10^{-15} s s^{-1})	2.3(8)	0.7(5)	$\cdots$
Mass ratio, $q \equiv m_1/m_2$	10.5(5)	8.1(2)	11.70(13)
Companion mass, m_2 ($M_\odot$)	0.16(2)	$0.181^{+0.008}_{-0.007}$	0.172(3)
Pulsar mass, m_1 ($M_\odot$)	1.64(22)	$1.46^{+0.06}_{-0.05}$	2.01(4)
$\delta X \equiv (q-1)/(q+1)$	0.826(8)	0.780(5)	0.843(2)
`Estimated Quantities`			
Upper limit of $\lvert\dot{x}\rvert$ (10^{-15} s s^{-1})	$\cdots$	$\cdots$	1.9
Upper limit of $\lvert\dot{\eta}\rvert$ (10^{-14} s^{-1})	0.25	0.12	2.7
Upper limit of $\lvert\dot{\kappa}\rvert$ (10^{-14} s^{-1})	0.23	0.12	2.7
`Derived Quantities Based on GR`			
Orbital inclination, i (deg)	52(4)	32.6(10)	40.2(6)
Advance of periastron, $\dot{\omega}$ (deg yr^{-1})	0.69(6)	1.57(5)	14.9(2)
Characteristic velocity, $\mathcal{V}_{\rm O}$ (km s^{-1})	308(13)	355(5)	590(4)

PSR J1738+0333

PSR J1738+0333 was discovered in 2001 in the high Galactic latitude survey with the 64-m Parkes telescope, and later regularly timed with the 305-m Arecibo telescope. It is one of MSPs known to be orbited by a WD companion bright enough for high-resolution spectroscopy. Accurate binary parameters and the 3 D spatial motion for the binary can be found in [36] and references therein. This small-eccentricity NS-WD binary has an orbital period of 8.5 hours, which, together with other well measured quantities, makes it a superb astrophysical laboratory to test gravity theories [36]. PSR J1738+0333 was used to constrain the PPN parameters, α_1 and α_2 [31]. The constraint on α_1 from this pulsar is the best limit up to now.

PSR J0348+0432

PSR J0348+0432 was discovered in a 350 MHz drift-scan survey using the Green Bank telescope. It has a spin period of 39 ms and an orbit period of 2.5 hours. The companion is a low-mass WD, whose spectra were later phase-resolved by optical observations from the Very Large Telescope [38]. The mass of WD was derived based on the comparison of optical observations with well-tested theoretical models of WDs, which gives $m_2 = 0.172 \pm 0.003\,M_\odot$. The mass ratio q was derived from the ratio of the WD radial velocity (from phase-resolved optical observations) to the pulsar radial velocity (from radio-timing observations). The mass ratio, along with the WD mass, leads to $m_1 = 2.01 \pm 0.04\,M_\odot$, that is the highest well-measured NS mass [38]. PSR J0348+0432 is a superb system for studies of equation of state of superdense nuclear matter, binary evolution, and tests of gravity theories. In [38], the agreement of its measured $\dot{P}_b$ with that from GR imposes stringent constraints on the parameter space of scalar-tensor theories. For studies here, it is worthy to mention that the periastron advance rate calculated in GR is $\dot{\omega} \simeq 15\,{\rm deg\,yr}^{-1}$ for PSR J0348+0432, which would have resulted in a rotation of the periastron for $\sim 55^\circ$ in $T_{\rm obs} \simeq 3.7$ years.

Small-eccentricity binary pulsars without theory-independent mass measurements

PSR J1802−2124

PSR J1802−2124 was discovered in the Parkes Multibeam Pulsar Survey in 2002. It is a 12.6 ms pulsar in a 16.8-hour orbit with a relatively massive WD companion. It is a useful example of the intermediate-mass class of binary pulsar systems, that provide interesting clues to binary evolution scenarios. The relatively large companion mass and its fortunately large orbital inclination angle produce a detectable Shapiro delay. It was measured through observations conducted at Parkes telescope, Green Bank telescope, and Nançay telescope [39]. The *shape* and *range* of Shapiro delay help to pin down the component masses in GR to be $m_1 = 1.24 \pm 0.11\,\mathrm{M}_\odot$ and $m_2 = 0.78 \pm 0.04\,\mathrm{M}_\odot$. See Table III for the timing solution of PSR J1802−2124 [39]. It is worthy mentioning that the precision for the orbital eccentricity has reached a level at $\sigma_e \sim \mathcal{O}(10^{-8})$.

PSR J0437−4715

PSR J0437−4715 is the brightest and nearest MSP, discovered at a Parkes survey at 430 MHz in 1993. It is also one of the most well-timed pulsars with a timing residual $\sim$ 200 ns [40]. Shapiro delay was detected in PSR J0437−4715. Moverover, because of its proximity, the secular change in the inclination angle of the orbit, due to its proper motion that gradually alters our line of sight to the orbital plane, was observed. It allows to break the ambiguity between i and $180^\circ - i$, and also determine the longitude of ascending node, Ω [42]. Therefore, the 3 D orbital geometry is fully determined for PSR J0437−4715. The most updated timing solution is presented in [40] based on 10 years of Parkes high-precision observations (see Table III). The very precison of this binary allowed to detect errors in the old Solar system ephemerides and place a stringent limit on the time variation of the gravitational constant [40]. For relevance here, the precision for the orbital eccentricity has reached a level at $\sigma_e \sim \mathcal{O}(10^{-9})$. PSR J0437−4715 is also one of the most important target in the PTA projects aiming at a detection of gravitational waves [41].

PSR B1855+09

PSR B1855+09 (a.k.a. PSR J1857+0943) was detected by Arecibo telescope in 1986. It is a binary pulsar with a 5.4 ms spin period in a nearly circular 12.3-day orbit with a helium WD companion. The WD companion was later detected optically by Keck and Hubble Space Telescope observations. Shapiro delay in this system was detected in early 1990's that revealed its nearly edge-on orbit ($i \sim 88^\circ$). It is the first detected Shapiro delay in pulsar binaries. Although LV tests in general require relativistic orbits, PSR B1855+09, with a relatively long orbital period, $P_\mathrm{b} \sim 12$ days, still provides some sensitivities due to its high-precision timing and a long timing baseline $T_\mathrm{obs} \gtrsim 20$ years. The updated timing solution [41] is presented in Table III.

PSR J1909−3744

PSR J1909−3744 was discovered during the Swinburne High Latitude Pulsar Survey using the Parkes telescope. It is a bianry MSP with a very small duty cycle in its pulse profile, that permits high-precision radio timing. The highly inclined orbit ($i \sim 86^\circ$) allowed the measurement of the relativistic Shapiro delay in PSR J1909−3744. A timing solution from 5 years of Parkes observations is presented in Table III, where the timing residual has reached a level less than 200 ns [41]. It is among the best timed pulsars that are being used to detect gravitational waves in PTAs.

Eccentric binary pulsars

PSR B1913+16

PSR B1913+16 (a.k.a. PSR J1915+1606 or the Hulse-Taylor pulsar) was the first binary pulsar discovered at the Arecibo Observatory. Since its discovery precision tests of gravity theories in the strong field were made feasible. The pulsar has a spin period of 59 ms and is in a 7.75-hour orbit. Follow-up radio timing observations verified Einstein's GR up to a precision of 0.2% (see [32] and references therein). The relativistic timing observables for PSR B1913+16 include the periastron advance rate $\dot{\omega}$, the "Einstein delay" in terms of the time dilation parameter, γ, and the shinkage of the orbit in terms of the time derivative of the orbital period, $\dot{P}_b$. The agreement of the predicted quadrupole damping effects in GR and the measured $\dot{P}_b$ value constitutes the first observational evidence of the existence of gravitational waves. The timing solution obtained from data taken at Arecibo telescope from 1981 to 2006 [32] is listed in Table IV. During such a time baseline, the periastron has already rotated out an angle $\sim 100^\circ$, that is the largest one in our binary samples.

PSR B1534+12

PSR B1534+12 (a.k.a. PSR J1537+1155) is a 38 ms pulsar in a 10.1-hour orbit discovered at the Arecibo Observatory. It has a high orbital inclination near to

TABLE III. Relevant parameters in LV tests for PSRs J1802−2124 [39], J0437−4715 [40], B1855+09, and J1909−3744 [41]. Parenthesized numbers represent the uncertainty in the last quoted digits. There is an ambiguity between i and $180^\circ - i$; only the value $i < 90^\circ$ is tabulated.

Pulsar	PSR J1802−2124	PSR J0437−4715	PSR B1855+09	PSR J1909−3744
`Observed Quantities`				
Observational span, $T_{\rm obs}$ (year)	~ 6 [39]	~ 10 [40]	~ 22 [41]	~ 5 [41]
Right ascension, α (J2000)	$18^{\rm h}02^{\rm m}05\overset{\rm s}{.}335576(5)$	$04^{\rm h}37^{\rm m}15\overset{\rm s}{.}814764(3)$	$18^{\rm h}57^{\rm m}36\overset{\rm s}{.}392909(7)$	$19^{\rm h}09^{\rm m}47\overset{\rm s}{.}4366120(4)$
Declination, δ (J2000)	$-21^\circ24'03''.649(2)$	$-47^\circ15'08''.62417(3)$	$09^\circ43'17''.2754(2)$	$-37^\circ44'14''.38013(2)$
Proper motion in α, μ_α (mas yr^{-1})	$-0.85(5)$	121.45(1)	$-2.64(2)$	$-9.510(4)$
Proper motion in δ, μ_δ (mas yr^{-1})	< 2.4	$-71.46(1)$	$-5.46(2)$	$-35.859(10)$
Spin period, P (ms)	12.6475935865227(3)	5.7574519243621(1)	5.36210054173545(3)	2.9471080681076399(5)
Orbital period, $P_{\rm b}$ (day)	0.698889243381(5)	5.741046(2)	12.32719(2)	1.533449474590(3)
Projected semimajor axis, x (lt-s)	3.7188533(5)	3.36669708(14)	9.230780(3)	1.89799106(4)
Eccentricity, e (10^{-5})	0.248(5)	1.9180(7)	2.170(3)	0.013(1)
Longitude of periastron, ω (deg)	20(2)	1.22(5)	276.5(1)	182(9)
Epoch of periastron, T_0 (MJD)	53452.673(4)	52009.8524(8)	50476.095(4)	53630.723214894(2)
$\eta \equiv e\sin\omega$ (10^{-7})	8.6(9)	···	···	$-0.04(20)$
$\kappa \equiv e\cos\omega$ (10^{-7})	23.2(4)	···	···	$-1.3(1)$
Shapiro delay parameter, s	0.984(2)	0.675(3)	0.9990(4)	0.9980(1)
Shapiro delay parameter, r (μs)	3.8(2)	1.25(9)	1.33(7)	1.04(1)
Longitude of ascending node, Ω (deg)	···	208(7)	···	···
`Estimated Quantities`				
Upper limit of $\lvert\dot{e}\rvert$ ($10^{-16}\,{\rm s}^{-1}$)	9.1	0.77	1.5	2.2
Upper limit of $\lvert\dot{x}\rvert$ ($10^{-15}\,{\rm s\,s}^{-1}$)	9.1	1.5	15	0.88
`Derived Quantities Based on GR`				
Pulsar mass, m_1 ($M_\odot$)	1.24(11)	1.76(20)	1.6(2)	1.53(2)
Companion mass, m_2 ($M_\odot$)	0.78(4)	0.254(18)	0.27(2)	0.212(2)
$\delta X \equiv (m_1 - m_2)/(m_1 + m_2)$	0.23(5)	0.75(3)	0.71(1)	0.757(1)
Inclination, i (deg)	79.9(6)	42.4(2)	87.5(5)	86.4(1)
Advance of periastron, $\dot{\omega}$ (deg yr^{-1})	0.58(2)	0.016(8)	0.0046(3)	0.141(1)
Characteristic velocity, $\mathcal{V}_{\rm O}$ (km s^{-1})	303(6)	150(5)	114(4)	222(1)

80°. Besides the $\dot{\omega}$-γ-$\dot{P}_b$ measurements, it also provided a measurement of the Shapiro delay that is caused by the curvature of spacetime near the companion star [33]. The timing solution obtained from data taken at the Arecibo telescope for about 12 years is listed in Table IV. The periastron has rotated out an angle $\sim 20^\circ$ during this time baseline. Stairs et al. [33] reported an upper limit for $\dot{e}$, $|\dot{e}| \lesssim 3 \times 10^{-15}$, and an upper limit for $\dot{x}$, $|\dot{x}| \lesssim 6.8 \times 10^{-13}\,{\rm s\,s}^{-1}$, which are valuable for studies here. Because more than one decade has passed since the publication of the current timing solution, new data will for sure provide even more constraining results.

PSR B2127+11C

PSR B2127+11C (a.k.a. PSR J2129+1210C or M15C) is a pulsar spinning at a period of 31 ms in the globular cluster M15 (a.k.a. NGC 7078). It was discovered at the Arecibo Observatory in 1989. The pulsar has an 8.0-hour orbit, and a companion suspected to be a NS. The Keplerian orbital parameters of PSR B2127+11C are nearly identical to those of PSR B1913+16 (see Table IV). Likewise, this pulsar also provided a $\dot{\omega}$-γ-$\dot{P}_b$ test, and GR passes the test within $\sim 3\%$ precision [35]. The most updated timing solution was obtained from about 12 years of data from the Arecibo Observatory, with a 5-year gap due to the update of the telescope [35].

PSR J0737−3039A/B

PSR J0737−3039A/B (a.k.a. the Double Pulsar) is the first and up to now the only system that composes two visible pulsars. It was discovered with the 64-m Parkes raido telescope. The orbital period is only 2.5 hours which makes the binary extremely relativistic with a characteristic velocity $\mathcal{V}_{\rm O} \simeq 625\,{\rm km\,s}^{-1}$ in GR. With a measurement of the mass ratio from the projected semimajor axes of two pulsars, as well the periastron advance

TABLE IV. Relevant parameters in LV tests for PSRs B1913+16 [32], B1534+12 [33], B2127+11C [35], and J0737−3039A [34]. Parenthesized numbers represent the uncertainty in the last quoted digits. There is an ambiguity between i and $180^\circ - i$; only the value $i < 90^\circ$ is tabulated.

Pulsar	PSR B1913+16	PSR B1534+12	PSR B2127+11C	PSR J0737−3039A
`Observed Quantities`				
Observational span, $T_{\rm obs}$ (year)	~ 25 [32]	~ 12 [33]	~ 12 [35]	~ 3 [34]
Right ascension, α (J2000)	$19^{\rm h}15^{\rm m}27\overset{\rm s}{.}99928(9)$	$15^{\rm h}37^{\rm m}09\overset{\rm s}{.}960312(10)$	$21^{\rm h}30^{\rm m}01\overset{\rm s}{.}2042(1)$	$07^{\rm h}37^{\rm m}51\overset{\rm s}{.}24927(3)$
Declination, δ (J2000)	$16^\circ06'27''.3871(13)$	$11^\circ55'55''.5543(2)$	$12^\circ10'38''.209(4)$	$-30^\circ39'40''.7195(5)$
Proper motion in α, μ_α ($\rm mas\,yr^{-1}$)	$-1.43(13)$	$1.32(3)$	$-1.3(5)$	$-3.3(4)$
Proper motion in δ, μ_δ ($\rm mas\,yr^{-1}$)	$-0.70(13)$	$-25.12(5)$	$-3.3(10)$	$2.6(5)$
Spin period, P (ms)	59.0300032180(5)	37.9044407982695(4)	30.52929614864(1)	22.699378599624(1)
Orbital period, $P_{\rm b}$ (day)	0.322997448911(4)	0.420737299122(10)	0.33528204828(5)	0.10225156248(5)
Eccentricity, e	0.6171334(5)	0.2736775(3)	0.681395(2)	0.0877775(9)
Projected semimajor axis, x (lt-s)	2.341782(3)	3.729464(2)	2.51845(6)	1.415032(1)
Longitude of periastron, ω (deg)	292.54472(6)	274.57679(5)	345.3069(5)	87.0331(8)
Epoch of periastron, T_0 (MJD)	52144.90097841(4)	50260.92493075(4)	50000.0643452(3)	53155.9074280(2)
Advance of periastron, $\dot\omega$ ($\rm deg\,yr^{-1}$)	4.226598(5)	1.755789(9)	4.4644(1)	16.89947(68)
Einstein delay parameter, γ (ms)	4.2992(8)	2.070(2)	4.78(4)	0.3856(26)
Shapiro delay parameter, s	···	0.975(7)	···	$0.99974^{+0.00016}_{-0.00039}$
Shapiro delay parameter, r (μs)	···	6.7(10)	···	6.21(33)
Intrinsic derivative of $P_{\rm b}$, $\dot P_{\rm b}^{\rm int}$ ($10^{-12}\,\rm s\,s^{-1}$)	$-2.396(5)$	$-0.174(11)$	$-3.95(13)$	$-1.252(17)$
Mass ratio, $q \equiv m_1/m_2$	···	···	···	1.0714(11)
`Estimated Quantities`				
Upper limit of $\lvert\dot e\rvert$ ($10^{-14}\,\rm s^{-1}$)	0.22	0.27	1.8	3.3
Upper limit of $\lvert\dot x\rvert$ ($10^{-13}\,\rm s\,s^{-1}$)	0.13	0.18	5.5	0.37
`Derived Quantities Based on GR`				
Pulsar mass, m_1 ($\rm M_\odot$)	1.4398(2)	1.3332(10)	1.358(10)	1.3381(7)
Companion mass, m_2 ($\rm M_\odot$)	1.3886(2)	1.3452(10)	1.354(10)	1.2489(7)
$\delta X \equiv (m_1 - m_2)/(m_1 + m_2)$	0.0181(1)	$-0.0045(5)$	0.001(5)	0.0345(4)
Inclination, i (deg)	47.194(7)	77.2(1)	50.1(4)	$88.69^{+0.50}_{-0.76}$
Characteristic velocity, $\mathcal{V}_{\rm O}$ ($\rm km\,s^{-1}$)	438.8390(4)	394.593(1)	427.426(7)	625.04(1)

rate, the Einstein delay, the Shapiro delay, and the orbital shinkage, it provided many tests of gravity theories just from one system [34]. GR were tested up to a precision of 0.05% by only using 3 years of data [34]. PSR J0737−3039A is the recycled pulsar in the binary and is the significantly better timed one. One notable quantity of its timing parameters is the very large periastron advance rate, $\dot\omega \simeq 17\,\rm deg\,yr^{-1}$, that has rotated the periastron by $\sim 50^\circ$ in 3 years.